Progress In Electromagnetics Research, Vol. 120, 293–307, 2011

BENDING ANALYSIS OF A DUAL-CORE PHOTONIC CRYSTAL FIBER

D. Chen [1, 2, *], G. Hu [1, 2], X. A. Liu [1, 2], B. Peng [1, 2], and G. Wu [1, 2]

[1]Institute of Information Optics, Zhejiang Normal University, Jinhua 321004, China

[2]Joint Research Laboratory of Optics of Zhejiang Normal University and Zhejiang University, Jinhua 321004, China

Abstract—A dual-core photonic crystal fiber (DC-PCF) is proposed, and bending characteristics of the DC-PCF are investigated. Two fiber cores are employed in the cross-section of the DC-PCF, which result in a mode coupling between the two fiber cores when the light propagates inside the DC-PCF. The mode coupling between two fiber cores of the DC-PCF is sensitive to the directional bending of the DC-PCF which essentially provides a method to achieve bending sensing. A DC-PCF-based bending sensor is proposed by injecting a broadband light into one fiber core of the DC-PCF on one side and detecting output spectrum from another fiber core of the DC-PCF on the other side. In our simulations, a parabola curve which shows the relationship between the wavelength shift of the transmission spectrum of the DC-PCF-based bending sensor and the bending curvature of the DC-PCF is presented.

1. INTRODUCTION

The appearance of photonic crystal fibers (PCFs) [1–10] with silica-air microstructure is a milestone in the history of optical fibers, which have achieved excellent optical properties in birefringence [11–16], dispersion [17–20], single polarization single mode [21–25], nonlinearity [26–30], and effective mode area [31–35] over the past several years. It is well known that PCFs have shown excellent performances in applications such as optical communications [36–38], fiber lasers [39–42], supercontinuum sources [43–46] and also fiber

Received 9 August 2011, Accepted 8 September 2011, Scheduled 9 September 2011

* Corresponding author: Daru Chen (daru@zjnu.cn).

sensors [47–56]. Fiber sensors based on PCFs have shown numerous advantages such as temperature insensitivity for strain sensing [49, 50], high sensitivity for gas sensing [51], biochemical sensing [52], refractive index sensing [53] and pressure sensing [54, 55], and the flexibility to form fiber sensors based on all-fiber Mach-Zehnder interferometers [56], which are mainly due to the remarkable flexibility in the fiber structure design of the PCF compared with the conventional optical fiber. It is worthy to note that besides the one-core PCF, multi-core PCFs including dual-core PCFs (DC-PCFs) have also been proposed for special applications. DC-PCFs have been designed for coupling inside PCFs [57–60], which can be used to achieve compact PCF couplers. Koshiba's group has proposed a wavelength MUX-DEMUX based on a DC-PCF [61], a polarization splitter based on a three-core PCF [62], a narrow band-pass filter [63] and a 1×4 power splitter [64] based on multi-core PCFs. Meanwhile, bending characteristics such as bending loss of one-core PCFs were reported in the past several years [65–68]. However, to the best of our knowledge, so far there has been no research on the bending characteristics of the DC-PCF.

In this paper, we introduce a DC-PCF with two fiber cores separated by one air hole in the cross-section. The mode coupling between the two fiber cores of the DC-PCF which is sensitive to the directional bending of the DC-PCF is investigated. We show that the mode coupling between two fiber cores of the DC-PCF essentially provides a method to achieve bending sensing based on the DC-PCF. A DC-PCF-based bending sensor is supposed to be achieved by injecting a broadband light into one fiber core of the DC-PCF on one side and detecting the output spectrum from another fiber core of the DC-PCF on the other side. A parabola curve for the wavelength shift of the transmission spectrum of the DC-PCF-based bending sensor and the bending curvature of the DC-PCF is presented.

2. STRUCTURE PRINCIPLE AND PERFORMANCE

Figure 1(a) shows the cross-section of the proposed DC-PCF. The DC-PCF is formed by a triangular lattice of circular air holes with two missing holes as two fiber cores (A and B) which are separated by one air hole. The hole pitch is Λ, which is 2 μm in this paper for bending analysis. The diameter of the air hole is d. To simplify analysis, refractive indices of the pure silica and air are assumed to be 1.45 and 1 (for the straight DC-PCF), respectively. A full-vector finite-element method (FEM) and anisotropic perfectly matched layers are used to investigate guided modes of the proposed DC-PCF. Due to the existence of the two fiber cores in the DC-PCF, here we show two kinds

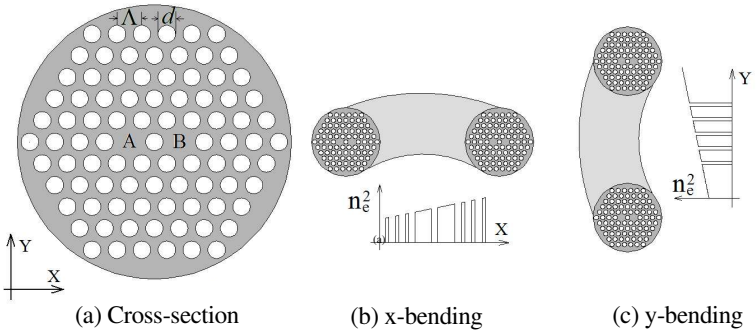

Figure 1. (a) Cross-section of the DC-PCF. (b) Schematic diagram for the x-bending DC-PCF. (c) Schematic diagram for the y-bending DC-PCF.

of bending DC-PCFs. Figs. 1(b) and (c) show schematic diagrams for the x-bending and y-bending DC-PCF, respectively. For the direct simulation of optical propagation in the bending DC-PCF, we need to employ an equivalent index profile ($n_e(x, y)$) in the cross-section of the DC-PCF, which is given by [68]

$$n_e^2(x, y) = n^2(x, y)\left(1 + \frac{2x}{R}\right) \tag{1}$$

for the x-bending DC-PCF, and

$$n_e^2(x, y) = n^2(x, y)\left(1 + \frac{2y}{R}\right) \tag{2}$$

for the y-bending DC-PCF, where R is the radius of curvature and $n(x, y)$ is the refractive index profile of the straight DC-PCF.

For a DC-PCF, two fiber cores in the cross-section lead to two waveguides inside the DC-PCF which accompany with a mode coupling. The coupling length which is defined as $L_c = \lambda/(2|n_e - n_o|)$ [69] is an important parameter for the mode coupling. Note that n_e and n_o are the effective indices of the even mode and the odd mode of the DC-PCF, and λ is the operation wavelength. To understand the mode coupling of the two fiber cores in the DC-PCF, we calculate the two basic modes (the even mode and the odd mode) of the straight DC-PCF with parameters of $\Lambda = 2\,\mu\text{m}$ and $d = 1.4\,\mu\text{m}$. For example, when the operation wavelength is $\lambda = 1550\,\text{nm}$, effective indices of the x-polarized even mode and the x-polarized odd mode are $n_e = 1.40458822$ and $n_o = 1.40429199$, respectively. Thus, the coupling length is $L_c = \lambda/(2|n_e - n_o|) = 2.62\,\text{mm}$, which means the optical power in the DC-PCF will be entirely transferred from one fiber

core to another after a length of 2.62 mm. For a bending DC-PCF, the coupling length is a function of the bending radius (or the bending curvature, which is reciprocal of the bending radius). Fig. 2 shows coupling length for the x-bending DC-PCF and the y-bending DC-PCF with different bending curvatures at the operation wavelength of 1550 nm. The coupling length for the y-bending DC-PCF almost remains the same when the bending curvature increases from 0 to $20\,\mathrm{m}^{-1}$, which is due to the fact that the symmetry of the index profile (shown by Eq. (2)) in the horizontal direction for the y-bending DC-PCF. However, the coupling length for the x-bending DC-PCF decreases when the bending curvature increases from 0 to $20\,\mathrm{m}^{-1}$, which is due to the change of the index profile (shown by Eq. (1)) in the horizontal direction for the x-bending DC-PCF. Thus, the coupling length of the DC-PCF is sensitive to the directional bending. In addition, the coupling length is also sensitive to the polarization state of the input light and the coupling length of the DC-PCF for the y-polarized light is larger than that for the x-polarized light.

As discussed above, the coupling length is an important parameter for the mode coupling which is sensitive to the bending curvature of the DC-PCF. However, the coupling length of the DC-PCF can not be simply measured by an equipment. Here we introduce a method based on spectrum measurement. For a DC-PCF with a length (z), suppose that the power of the injected light on the input side of the fiber core-A and the fiber core-B is 1 and 0, respectively. According to the conventional coupled-mode theory [69–73], the output power on the output side of the fiber core-A and the fiber core-B of the DC-PCF

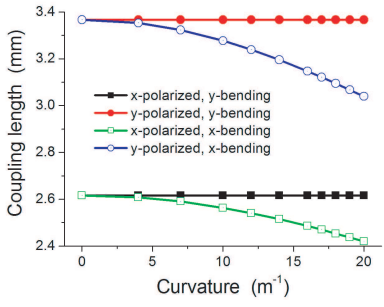

Figure 2. Coupling length for the x-bending DC-PCF and the y-bending DC-PCF with different bending curvature.

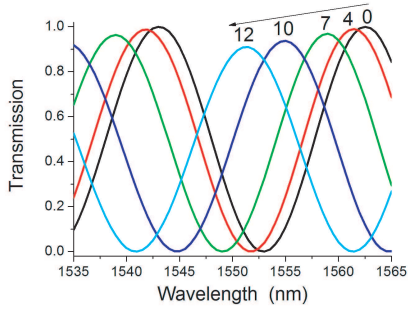

Figure 3. Output spectra (from fiber core-B) of the 10-cm DC-PCF when the (x-) bending curvature is 0, 4, 7, 10, and $12\,\mathrm{m}^{-1}$, respectively.

can be given by

$$P_1(z,\lambda) = \cos^2(Sz) + \cos^2(\eta)\sin^2(Sz) \tag{3}$$

and

$$P_2(z,\lambda) = \sin^2(\eta)\sin^2(Sz), \tag{4}$$

respectively. The maximum power transferred from the fiber core-A to the fiber core-B is

$$P_2|_{\max} = \sin^2(\eta) \tag{5}$$

which occurs at the coupling length $z = L_c = \pi/(2S)$. Note that we have

$$S = |n_e - n_o|\pi/\lambda, \tag{6}$$

$$S = \sqrt{\delta^2 + \kappa^2}, \tag{7}$$

$$\tan(\eta) = \delta/\kappa, \tag{8}$$

and

$$\delta = |n_a - n_b|\pi/\lambda, \tag{9}$$

where n_a and n_b are the effective index of the individual fiber core-A and the individual fiber core-B, respectively. For a straight DC-PCF, we have $\delta = 0$ since the fiber core-A and the fiber core-B are symmetrical in the DC-PCF. Thus, Eqs. (3), (4) and (5) can be rewritten as

$$P_1(z,\lambda) = \cos^2(Sz), \tag{10}$$

$$P_2(z,\lambda) = \sin^2(Sz), \tag{11}$$

and

$$P_2|_{\max} = 1. \tag{12}$$

We calculate the transmission spectrum (from fiber core-A to fiber core-B) of the 10-cm DC-PCF when the (x-) bending curvature is 0, 4, 7, 10, and 12 m^{-1}, respectively, which are shown in Fig. 3. The sine-like transmission spectrum is due to $P_2(z,\lambda)$ described in Eq. (4), where $|n_e - n_o|$ slowly varies for the operation wavelength. The period of the sine-like transmission spectrum is corresponding to the length of the DC-PCF, which does not affect the wavelength shift corresponding to the bending curvature of the DC-PCF. A blue shift of the output spectrum of the 10-cm DC-PCF together with the decrease of the maximum power transferred from the fiber core-A to the fiber core-B is observed when the bending curvature of the DC-PCF increases. This could also be indicated by the mode profiles of the even mode and the odd mode of the DC-PCF. Fig. 4 shows the mode profiles (electric field) for (a) the even mode and (b) the odd mode of the straight DC-PCF, and normalized amplitude of the electric field for (c) the even

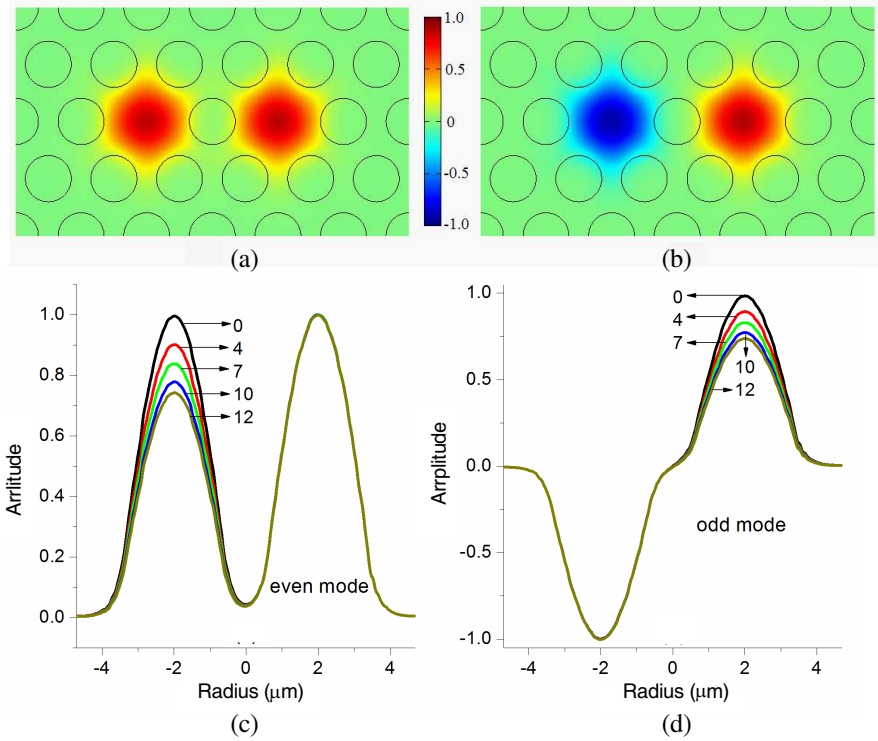

Figure 4. Mode profiles (electric field) for (a) the even mode and (b) the odd mode of the straight DC-PCF; Normalized amplitude of the electric field for (c) the even mode and (d) the odd mode of the x-bending DC-PCF with bending curvature of 0, 4, 7, 10, and 12 m^{-1}, respectively.

mode and (d) the odd mode of the x-bending DC-PCF with a bending curvature of 0, 4, 7, 10, and 12 m^{-1}, respectively.

The dependence between the transmission spectrum of the 10-cm DC-PCF and the bending curvature indicates a method to achieve bending sensing. Fig. 5 shows the two parabola curves for the wavelength shift of the peak wavelength of the transmission spectrum (from fiber core-A to fiber core-B) of the 10-cm DC-PCF and the bending curvature for the x-polarized light and y-polarized light. Thus, a DC-PCF-based bending sensor can be achieved by injecting broadband polarized light into one fiber core of DC-PCF on one side and detecting output spectrum from another fiber core of the DC-PCF on the other side. Our calculations show that the DC-PCF-

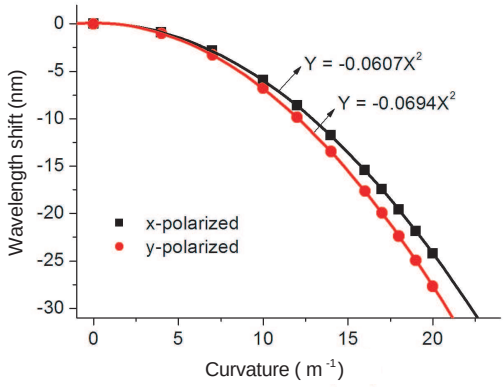

Figure 5. Wavelength shift of the peak wavelength of the transmission spectrum (from fiber core-A to fiber core-B) of the 10-cm DC-PCF and the bending curvature for the injected x-polarized light and injected y-polarized light.

based bending sensor can have a measurement range of at least $20\,\mathrm{m}^{-1}$ and a sensitivity of $1.388\,\mathrm{nm/(m^{-1})}$ ($2.776\,\mathrm{nm/(m^{-1})}$) for the bending curvature $10\,\mathrm{m}^{-1}$ ($20\,\mathrm{m}^{-1}$) when we consider a broadband y-polarized light. Note that the sensitivity ($S = \Delta\lambda/\Delta c$) of a bending sensor is defined as the ratio of the wavelength change and the bending curvature change.

When the DC-PCF is used for bending curvature measurement, the confinement loss of the DC-PCF should also be evaluated. The calculated confinement loss of the DC-PCF with parameters of $\Lambda = 2\,\mu\mathrm{m}$ and $d = 1.4\,\mu\mathrm{m}$ has the order of magnitude of $10^{-5}\,\mathrm{dB/km}$ when the bending curvature of the DC-PCF is in the range from 0 to 100 m^{-1}. Thus the confinement loss of the 10-cm DC-PCF used for bending sensing can be ignored since it is much smaller than the loss of a 10-cm standard single mode fiber. The calculated confinement loss of DC-PCFs with parameters of ($\Lambda = 2.2\,\mu\mathrm{m}$ and $d = 1.4\,\mu\mathrm{m}$) or ($\Lambda = 2\,\mu\mathrm{m}$ and $d = 1.3\,\mu\mathrm{m}$) has the order of magnitude of $10^{-4}\,\mathrm{dB/km}$ or $10^{-3}\,\mathrm{dB/km}$ when the bending curvature of DC-PCFs is in the range from 0 to $100\,\mathrm{m}^{-1}$, which indicate the confinement loss of these DC-PCFs can also be ignored when they are used for bending sensing. The calculate wavelength shifts of three types of 10-cm DC-PCFs with parameters of ($\Lambda = 2\,\mu\mathrm{m}$ and $d = 1.4\,\mu\mathrm{m}$), ($\Lambda = 2.2\,\mu\mathrm{m}$ and $d = 1.4\,\mu\mathrm{m}$) or ($\Lambda = 2\,\mu\mathrm{m}$ and $d = 1.3\,\mu\mathrm{m}$) for the bending curvature of 4 are 1.0 nm, 1.9 nm, and 0.9 nm, respectively. Our calculations show that DC-PCF with a larger hole pitch and a larger air hole size

can achieve a higher sensitivity of the DC-PCF-based bending sensor, which, however may lead to larger confinement loss and smaller sensing range. The sensing range of the proposed bending sensor is limited firstly to the confinement loss of the bending DC-PCF and secondly to the broadband light source and the optical spectrum analyzer. For the proposed bending sensor based on a 10-cm DC-PCF with parameters of ($\Lambda = 2\,\mu m$ and $d = 1.4\,\mu m$) has a sensing range from 0 to $100\,m^{-1}$, when the broadband light source and the optical spectrum analyzer can support its application.

3. DISCUSSION AND CONCLUSION

The fabrication of the DC-PCF will be easy by using the current PCF fabrication techniques available. Several multi-one PCFs have been fabricated and demonstrated [32, 42] recently. However, an imperfect fabrication of the DC-PCF will results in difficulties for bending sensing application. The operation principle of a DC-PCF-based bending sensor is due to the mode coupling between two fiber cores of the DC-PCF. When the size of a designed DC-PCF is changed during the fabrication, the working curve (parabola curve in Fig. 5) will also be changed, which may lead to a different sensitivity and sensing range. When the symmetry of the designed DC-PCF is changed during the fabrication, the zero bending curvature point in the working curve will shift. Thus, a DC-PCF-based bending sensor should be calibrated before it is practically used.

A challenging technique for the DC-PCF based sensor is how to connect the DC-PCF to the light source or the optical spectrum analyzer, since the fiber core size and the distance between the two fiber cores of the DC-PCF is too small compared with the fiber core of the single mode fiber. It may be overcome by firstly splicing a one-core PCF to the DC-PCF where the fiber cores of the one-core PCF and the DC-PCF are the same, and then splicing the single mode fiber to the one-core PCF. Chiang *et al.* has also provided useful method for the connection between the PCF and the single mode fiber [74].

Considering the index change effect for pressure, strain, and temperature, the DC-PCF can also be designed for pressure sensing, strain sensing, temperature sensing. However, previously reported works have shown that the PCF-based sensor is not very sensitive to temperature [49, 50] and pressure [47, 48, 54]. Only extreme high temperature or high pressure can be an effective external perturbation for the proposed DC-PCF-based bending sensor. In most instances, the DC-PCF-based bending sensor can work well without external perturbations.

In conclusion, we have analyzed a bending DC-DCF with two fiber cores separated by one air hole in the cross-section. The mode coupling of two fiber cores inside the DC-PCF has been introduced by considering the fiber bending. Simulations have shown we can achieve bending sensing by measuring the wavelength shift of the output spectrum at one fiber core on output side of the DC-DCF with a fixed length when the broadband polarized light is injected into another fiber core on input side of the DC-DCF. The performance of a 10-cm DC-PCF-based bending sensor has been presented.

ACKNOWLEDGMENT

This work is supported by the National Natural Science Foundation of China under project (No. 61007029), The Projects of Zhejiang Province (No. 2011C21038 and No. 2010R50007) and the Program for Science and Technology Innovative Research Team in Zhejiang Normal University.

REFERENCES

1. Knight, J. C., J. Broeng, T. A. Birks, and P. St. J. Russell, "Photonic band gap guidance in optical fibers," *Science*, Vol. 282, 1476–1478, 1998.
2. Knight, J. C. and P. S. J. Russell, "Photonic crystal fibers: New way to guide light," *Science*, Vol. 296, 276–277, 2002.
3. Knight, J. C., "Photonic crystal fibers," *Nature*, Vol. 424, 847–851, 2003.
4. Nozhat, N. and N. Granpayeh, "Specialty fibers designed by photonic crystals," *Progress In Electromagnetics Research*, Vol. 99, 225–244, 2009.
5. Makoui, S., M. Savadi-Oskouei, A. Rostami, and Z. D. Koozehkanani, "Dispersion flattened optical fiber design for large bandwidth and high-speed optical communications using optimization technique," *Progress In Electromagnetics Research B*, Vol. 13, 21–40, 2009.
6. Wu, J.-J., D. Chen, K.-L. Liao, T.-J. Yang, and W.-L. Ouyang, "The optical properties of Bragg fiber with a fiber core of 2-dimension elliptical-hole photonic crystal structure," *Progress In Electromagnetics Research Letters*, Vol. 10, 87–95, 2009.
7. Chau, Y.-F., C.-Y. Liu, H.-H. Yeh, and D. P. Tsai, "A Comparative study of high birefringence and low confinement loss photonic crystal fiber employing elliptical air holes in fiber

cladding with tetragonal lattice," *Progress In Electromagnetics Research B*, Vol. 22, 39–52, 2010.

8. Karimi M. and F. E. Seraji, "Effects of geometry on amplification property of erbium doped holey fiber amplifiers using scalar effective index method," *Progress In Electromagnetics Research B*, Vol. 19, 385–403, 2010.
9. Chen, D. and H. Chen, "Highly birefringent low-loss terahertz waveguide: Elliptical polymer tube," *Journal of Electromagnetic Waves and Applications*, Vol. 24, No. 11–12, 1553–1562, 2010.
10. Chen, D., M.-L. V. Tse, and H.-Y. Tam, "Optical properties of photonic crystal fibers with a fiber core of arrays of subwavelength circular air holes: Birefringence and dispersion," *Progress In Electromagnetics Research*, Vol. 105, 193–212, 2010.
11. Ortigosa-Blanch, A., J. C. Knight, W. J. Wadsworth, J. Arriaga, B. J. Mangan, T. A. Birks, and P. St. J. Russell, "Highly birefringent photonic crystal fibers," *Opt. Lett.*, Vol. 25, No. 18, 1325–1327, 2000.
12. Steel, M. J. and R. M. Osgood, "Elliptical-hole photonic crystal fibers," *Opt. Lett.*, Vol. 26, No. 4, 229–231, 2001.
13. Chen, D. and L. Shen, "Highly birefringent elliptical-hole photonic crystal fibers with double defect," *J. Lightw. Technol.*, Vol. 25, No. 9, 2700–2705, 2007.
14. Chen, D. and L. Shen, "Ultrahigh birefringent photonic crystal fiber with ultralow confinement loss," *IEEE Photon. Technol. Lett.*, Vol. 19, No. 4, 185–187, 2007.
15. Beltrán-Mejía, F., G. Chesini, E. Silvestre, A. K. George, J. C. Knight, and C. M. Cordeiro, "Ultrahigh-birefringent squeezed lattice photonic crystal fiber with rotated elliptical air holes," *Opt. Lett.*, Vol. 35, No. 4, 544–546, 2010.
16. Chen, D. and G. Wu, "Highly birefringent photonic crystal fiber based on a double-hole unit," *Appl. Opt.*, Vol. 49, No. 9, 1682–1686, 2010.
17. Singh, V. and D. Kumar, "Modal dispersion characteristics of a Bragg fiber having plasma in the cladding regions," *Progress In Electromagnetics Research*, Vol. 89, 167–181, 2009.
18. Saitoh, K., M. Koshiba, T. Hasegawa, and E. Sasaoka, "Chromatic dispersion control in photonic crystal fibers: Application to ultra-flattened dispersion," *Opt. Express*, Vol. 11, 843–852, 2003.
19. Yang, S., Y. Zhang, X. Peng, Y. Lu, S. Xie, J. Li, W. Chen, Z. Jiang, J. Peng, and H. Li, "Theoretical study and experimental fabrication of high negative dispersion photonic crystal fiber with

large area mode field," *Opt. Express*, Vol. 14, 3015–3023, 2006.

20. Wong, G. K. L., L. Zang, M. S. Kang, and P. St. J. Russell, "Measurement of group-velocity dispersion of Bloch modes in photonic-crystal-fiber rocking filters," *Opt. Lett.*, Vol. 35, No. 23, 3982–3984, 2010.
21. Birks, T. A., J. C. Knight, and P. St. J. Russel, "Endlessly single-mode photonic crystal fiber," *Opt. Lett.*, Vol. 22, No. 13, 961–963, 1997.
22. Saitoh, K. and M. Koshiba, "Single-polarization single-mode photonic crystal fibers," *IEEE Photon. Technol. Lett.*, Vol. 15, No. 10, 1384–1340, 2003.
23. Kubota, H., S. Kawanishi, S. Koyanagi, M. Tanaka, and S. Yamaguchi, "Absolutely single polarization photonic crystal fiber," *IEEE Photon. Technol. Lett.,* Vol. 16, 182–184, 2004.
24. Hu, D. J. J., P. Shum, C. Lu, X. Yu, G. Wang, and G. Ren, "Holey fiber design for single-polarization single-mode guidance," *Appl. Opt.,* Vol. 48, No. 20, 4038–4043, 2009.
25. Wang, L., S. Lou, W. Chen, and H. Li, "Design of a single-polarization single-mode photonic crystal fiber with a near-Gaussian mode field and wide bandwidth," *Appl. Opt.*, Vol. 49, No. 32, 6196–6200, 2010.
26. Knight, J. C. and D. V. Skryabin, "Nonlinear waveguide optics and photonic crystal fibers," *Opt. Express,* Vol. 15, No. 23, 15365–15376, 2007.
27. Welch, M. G., K. Cook, R. A. Correa, F. Gérôme, W. J. Wadsworth, A. V. Gorbach, D. V. Skryabin, and J. C. Knight, "Solitons in hollow core photonic crystal fiber: Engineering nonlinearity and compressing pulses," *J. Lightwave Technol.,* Vol. 27, No. 11, 1644–1652, 2009.
28. Bao, H. and M. Gu, "Reduction of self-phase modulation in double-clad photonic crystal fiber for nonlinear optical endoscopy," *Opt. Lett.,* Vol. 34, No. 2, 148–150, 2009.
29. Wang, Y., X. Zhang, X. Ren, L. Zheng, X. Liu, and Y. Huang, "Design and analysis of a dispersion flattened and highly nonlinear photonic crystal fiber with ultralow confinement loss," *Appl. Opt.,* Vol. 49, No. 3, 292–297, 2010.
30. Raja, R. V. J., A. Husakou, J. Hermann, and K. Porsezian, "Supercontinuum generation in liquid-filled photonic crystal fiber with slow nonlinear response," *J. Opt. Soc. Am. B,* Vol. 27, No. 9, 1763–1768, 2010.

31. Mortensen, N. A., M. D. Nielsen, J. R. Folkenberg, A. Petersson, and H. R. Simonsen, "Improved large-mode-area endlessly single-mode photonic crystal fibers," *Opt. Lett.,* Vol. 28, No. 6, 393–395, 2003.
32. Michaille, L., D. M. Taylor, C. R. Bennett, T. J. Shepherd, and B. G. Ward, "Characteristics of a Q-switched multicore photonic crystal fiber laser with a very large mode field area," *Opt. Lett.*, Vol. 33, No. 1, 71–73, 2008.
33. Nodop, D., C. Jauregui, D. Schimpf, J. Limpert, and A. Tünermann, "Efficient high-power generation of visible and mid-infrared light by degenerate four-wave-mixing in a large-mode-area photonic-crystal fiber," *Opt. Lett.*, Vol. 34, No. 22, 3499–3501, 2009.
34. Lefrançois, S., K. Kieu, Y. Deng, J. D. Kafka, and F. W. Wise, "Scaling of dissipative soliton fiber lasers to megawatt peak powers by use of large-area photonic crystal fiber," *Opt. Lett.*, Vol. 35, No. 10, 1569–1571, 2010.
35. Baumgartl, M., F. Jansen, F. Stutzki, C. Jauregui, B. Ortaç, J. Limpert, and A. Tünnermann, "High average and peak power femtosecond large-pitch photonic-crystal-fiber laser," *Opt. Lett.*, Vol. 36, No. 2, 244–246, 2011.
36. Astar, W., C.-C. Wei, Y.-J. Chen, J. Chen, and G. M. Carter, "Polarization-insensitive, 40 Gb/s wavelength and RZ-OOK-to-RZ-BPSK modulation format conversion by XPM in a highly nonlinear PCF," *Opt. Express,* Vol. 16, No. 16, 12039–12049, 2008.
37. Matsui, T., K. Nakajima, and C. Fukai, "Applicability of photonic crystal fiber with uniform air-hole structure to high-speed and wide-band transmission over conventional telecommunication bands," *J. Lightwave Technol.,* Vol. 27, No. 23, 5410–5416, 2009.
38. Wang, J., H. Miao, S. Song, and R. Zheng, "Study on compensating methods of transmission system at 40 Gb/s in photonic crystal fiber," *Chin. Opt. Lett.,* Vol. 8, No. 5, 471–473, 2010.
39. Limpert, J., T. Schreiber, S. Nolte, H. Zellmer, T. Tunnermann, R. Iliew, F. Lederer, J. Broeng, G. Vienne, A. Petersson, and C. Jakobsen, "High-power air-clad large-mode-area photonic crystal fiber laser," *Opt. Express,* Vol. 11, No. 7, 818–823, 2003.
40. Liu, X., X. Zhou, X. Tang, J. Ng, J. Hao, T. Chai, E. Leong, and C. Lu, "Switchable and tunable multiwavelength erbium-doped fiber laser with fiber Bragg grating and photonic crystal fiber," *IEEE Photon. Technol. Lett.,* Vol. 17, No. 8, 1626–1628, 2005.

41. Chen, D., "Stable multi-wavelength erbium-doped fiber laser based on photonic crystal fiber Sagnac loop filter," *Laser Phys. Lett.,* Vol. 4, No. 6, 437–439, 2007.
42. Fang, X., M. Hu, C. Xie, Y. Song, L. Chai, and C. Wang, "High pulse energy mode-locked multicore photonic crystal fiber laser," *Opt. Lett.,* Vol. 36, No. 6, 1005–1007, 2011.
43. Zhu, Z. and T. G. Brown, "Polarization properties of supercontinuum spectra generated in birefringent photonic crystal fibers," *J. Opt. Soc. Am. B*, Vol. 21, No. 2, 249–257, 2004.
44. Kudlinski, A., G. Bouwmans, O. Vanvincq, Y. Quiquempois, A. Le Rouge, L. Bigot, G. Mélin, and A. Mussot, "White-light cw-pumped supercontinuum generation in highly GeO_2-doped-core photonic crystal fibers," *Opt. Lett.,* Vol. 34, No. 23, 3631–3633, 2009.
45. Dudley, J. M. and J. R. Taylor, "Ten years of nonlinear optics in photonic crystal fibre," *Nature Photonics*, Vol. 3, 85–90, 2009.
46. Hooper, L. E., P. J. Mosley, A. C. Muir, W. J. Wadsworth, and J. C. Knight, "Coherent supercontinuum generation in photonic crystal fiber with all-normal group velocity dispersion," *Opt. Express,* Vol. 19, No. 6, 4902–4907, 2011.
47. Chen, D., G. Hu, M. L. V. Tse, H. Y. Tam, and L. Gao, "Dual-core side-hole fiber for pressure sensing based on intensity detection," *Journal of Electromagnetic Waves Applications,* Vol. 25, Nos. 5–6, 775–784, 2011.
48. Chen, D., M.-L. V. Tse, C. Wu, G. Hu, and H.-Y. Tam, "Highly birefringent four-hole fiber for pressure sensing," *Progress In Electromagnetics Research,* Vol. 114, 145–158, 2011.
49. Dobb, H., K. Kalli, and D. J. Webb, "Temperature-insensitive long period grating sensors in photonic crystal fibre," *Eletron. Lett.*, Vol. 40, No. 11, 657–658, 2004.
50. Dong, X. and H. Y. Tam, "Temperature-insensitive strain sensor with polarization-maintaining photonic crystal fiber based on Sagnac interferometer," *Appl. Phys. Lett.,* Vol. 90, No. 15, 151113–151115, 2007.
51. Ritari, T., J. Tuominen, H. Ludvigsen, J. C. Petersen, T. Sørensen, T. P. Hansen, and H. R. Simonsen, "Gas sensing using air-guiding photonic crystal bandgap fibers," *Opt. Express,* Vol. 12, No. 17, 4080–4087, 2004.
52. Rindorf, L., J. B. Jensen, M. Dufva, L. H. Pedersen, P. T. Høiby, and O. Bang, "Photonic crystal fiber long-period gratings for biochemical sensing," *Opt. Express*, Vol. 14, No. 18, 8224–48231,

2006.

53. Wu, D. K. C., B. T. Kuhlmey, and B. J. Eggleton, "Ultrasensitive photonic crystal fiber refractive index sensor," *Opt. Lett.,* Vol. 34, No. 3, 322–324, 2009.
54. Fu, H. Y., H. Y. Tam, L. Y. Shao, X. Dong, P. K. A. Wai, C. Lu, and S. K. Khijwania, "Pressure sensor realized with polarization-maintaining photonic crystal fiber-based Sagnac interferometer," *Appl. Opt.,* Vol. 47, No. 15, 2835–2839, 2008.
55. Kim, H. M., T. H. Kim, B. Kim, and Y. Chung, "Enhanced transverse load sensitivity by using a highly birefringent photonic crystal fiber with larger air holes on one axis," *Appl. Opt.,* Vol. 49, No. 20, 3841–3845, 2010.
56. Choi, H. Y., M. J. Kim, and B. H. Lee, "All-fiber mach-zehnder type interferometers formed in photonic crystal fiber," *Opt. Express,* Vol. 15, No. 9, 5711–5780, 2007.
57. Fogli, F., L. Saccomandi, P. Bassi, G. Bellance, and S. Trillo, "Full vectorial BMP modeling of index-guiding photonic crystal fibers and couplers," *Opt. Express,* Vol. 10, No. 1, 54–59, 2002.
58. Lee, B. H., J. B. Eom, J. Kim, D. S. Moon, and U.-C Paek, "Photonic crystal fiber coupler," *Opt. Lett.,* Vol. 27, No. 10, 812–814, 2002.
59. Zhang, L. and C. Yang, "Polarization-dependent coupling in twin-core photonic crystal fibers," *J. Lightwave Technol.,* Vol. 22, No. 5, 1367–1373, 2004.
60. Lagsgaard, J., O. Bang, and A. Bjarklev, "Photonic crystal fiber design for broadband directional coupling," *Opt. Lett.,* Vol. 29, No. 21, 2473–2475, 2004.
61. Saitoh, K., Y. Sato, and M. Koshiba, "Coupling characteristics of dual-core photonic crystal fiber couplers," *Opt. Express,* Vol. 11, No. 24, 3188–3195, 2003.
62. Saitoh, K., Y. Sato, and M. Koshiba, "Polarization splitter in three-core photonic crystal fibers," *Opt. Express,* Vol. 12, No. 17, 3940–3946, 2004.
63. Saitoh, K., N. J. Florous, M. Koshiba, and M. Skorobogatiy, "Design of narrow band-pass filters based on the resonant-tunneling phenomenon in multi-core photonic crystal fibers," *Opt. Express,* Vol. 13, No. 25, 10327–10335, 2005.
64. Varshney, S. K., K. Saitoh, R. K. Sinha, and M. Koshiba, "Coupling characteristics of multicore photonic crystal fiber-based 1×4 power splitters," *J. Lightwave Technol.,* Vol. 27, No. 12, 2062–2068, 2009.

65. Nielsen, M. D., N. A. Mortensen, and J. R. Folkenberg, "Reduced microdeformation attenuation in large-mode-area photonic crystal fibers for visible applications," *Opt. Lett.*, Vol. 28, No. 18, 1645–1647, 2003.
66. Nielsen, M., N. Mortensen, M. Albertsen, J. Folkenberg, A. Bjarklev, and D. Bonacinni, "Predicting macrobending loss for large-mode area photonic crystal fibers," *Opt. Express,* Vol. 12, No. 8, 1775–1779, 2004.
67. Olszewski, J., M. Szpulak, and W. Urbanczyk, "Effect of coupling between fundamental and cladding modes on bending losses in photonic crystal fibers," *Opt. Express,* Vol. 13, No. 16, 6015–6022, 2005.
68. Vu, N. H., I.-K. Hwang, and Y.-H. Lee, "Bending loss analyses of photonic crystal fibers based on the finite-difference time-domain method," *Opt. Lett.,* Vol. 33, No. 2, 119–121, 2008.
69. Huang, W. P., "Coupled-mode theory for optical waveguides: An overview," *J. Opt. Soc. Am. A*, Vol. 11, No. 3, 963–983, 1994.
70. Sun, N.-H., J.-J. Liau, Y.-W. Kiang, S.-C. Lin, R.-Y. Ro, J.-S. Chiang, and H.-W. Chang, "Numerical analysis of apodized fiber Bragg gratings using coupled mode theory," *Progress In Electromagnetics Research*, Vol. 99, 289–306, 2009.
71. Liau, J.-J., N.-H. Sun, S.-C. Lin, R.-Y. Ro, J.-S. Chiang, C.-L. Pan, and H.-W. Chang, "A new look at numerical analysis of uniform fiber Bragg gratings using coupled mode theory," *Progress In Electromagnetics Research*, Vol. 93, 385–401, 2009.
72. Liu, Y. and W.-B. Dou, "Mutually-tapped coupling between combline resonator pairs for ultra-wideband (UWB) filter realization," *Journal of Electromagnetic Waves and Applications*, Vol. 23, No. 8–9, 1165–1172, 2009.
73. Li, J., J. Wang, and F. Jing, "Improvement of coiling mode to suppress higher-order-modes by considering mode coupling for large-mode-area fiber laser," *Journal of Electromagnetic Waves and Applications*, Vol. 24, No. 8–9, 1113–1124, 2010.
74. Chiang, J.-S., N.-H. Sun, S.-C. Lin, and W.-F. Liu, "Analysis of an ultrashort PCF-based polarization splitter," *J. Lightwave Technol.*, Vol. 28, No. 5, 707–713, 2010.